# Iridanonaborane Chemistry: Preparation and Characterization of some *arachno*-4-Iridanonaboranes by Nuclear Magnetic Resonance Spectroscopy and Single-crystal *X*-Ray Diffraction Analysis †

**Jonathan Bould, Janet E. Crook, Norman N. Greenwood, and John D. Kennedy**
*Department of Inorganic and Structural Chemistry, University of Leeds, Leeds LS2 9JT*

The *nido* anion $[B_9H_{12}]^-$ reacts rapidly with an equimolar quantity of *trans*-$[Ir(CO)Cl(PMe_3)_2]$ at room temperature to produce the new, colourless, nine-vertex *arachno*-iridanonaboranes $[(HIrB_8H_{12})(CO)(PMe_3)_2]$ (1; 30% yield) and $[(HIrB_8H_{11}Cl)(CO)(PMe_3)_2]$ (2; 7% yield), together with the known yellow ten-vertex *nido*-$[6,6,6\text{-}H(PMe_3)_2\text{-}6\text{-}IrB_9H_{13}]$. Similar compounds are formed, although in much smaller yields, when *arachno*-$[B_9H_{14}]^-$ is used instead of *nido*-$[B_9H_{12}]^-$. Single-crystal *X*-ray diffraction studies show the detailed structure of (2) to be [1-Cl-*sym*-4,4,4,4-(CO)-*endo*-H-*cis*-$(PMe_3)_2$-*arachno*-4-$IrB_8H_{11}$]. Comparative n.m.r. spectroscopy ($^{31}P$, $^{11}B$, and $^1H$) shows that compound (1) has the configuration [*asym*-4,4,4,4-(CO)-*endo*-H-*cis*-$(PMe_3)_2$-*arachno*-4-$IrB_8H_{12}$]. Minor products of the reaction (≤1%) include a third new *arachno*-iridanonaborane [*sym*-4,4,4,4-*endo*-H-*mer*-$(PMe_3)_3$-4-$IrB_8H_{12}$] (3) and the previously reported five-vertex *arachno*-iridaborane-[1,1,1-$(CO)(PMe_3)_2$-*arachno*-1-$IrB_4H_9$]. The nine-vertex compounds all have the gross *arachno* nonaborane structure of *iso*-$B_9H_{15}$ similar to that of the platinum analogue $[(PtB_8H_{12})(PMe_2Ph)_2]$, but there are differences in the detail of the borane-to-metal bonding, which have important wider implications. The *arachno*-iridanonaboranes may be regarded as octahedral complexes of $d^6$ iridium(III).

It has previously been found that simple iridium(I) compounds such as *trans*-$[Ir(CO)Cl(PPh_3)_2]$ react readily with a variety of borane anions such as $[B_3H_8]^-$, $[B_5H_8]^-$, $[B_6H_9]^-$, $[B_9H_{14}]^-$, and $[B_{10}H_{10}]^{2-}$: generally an oxidative insertion of the metal atom to form iridium(III) or iridium(V) metallaborane species occurs, and this is often accompanied by condensation and/or cluster degradation reactions which result in a number of novel or otherwise interesting structural types.[1-9] As a continuation of these studies, we now report the results of work on the isolation and characterization of a series of nine-vertex *arachno*-iridanonaboranes which arise from the reaction of *trans*-$[Ir(CO)Cl(PMe_3)_2]$ with the *nido*-nonaborane anion $[B_9H_{12}]^-$. Some preliminary [10] and incidental [4] aspects of this work have been reported previously. In this work the conventional I.U.P.A.C. recommended [11,12] numbering systems are used for the clusters.

## Results and Discussion

We have previously described the reaction of the *arachno*-$[B_9H_{14}]^-$ anion with *trans*-$[Ir(CO)Cl(PMe_3)_2]$ to give small yields of the ten-vertex *nido*-iridadecaborane species $[(HIrB_9H_{13})(PMe_3)_2]$.[5] The major product of the reaction was the well known *arachno*-nonaborane compound $B_9H_{13}(PMe_3)$ but, in addition, trace quantities of other species were detected which were tentatively identified as nine-vertex *arachno*-iridanonaboranes. We have now found that these are indeed *arachno*-iridanonaboranes, and that they can be obtained in much higher yield from reactions involving the *nido* nine-vertex anion $[B_9H_{12}]^-$: the identity of the products with those from the $[B_9H_{14}]^-$ reaction was confirmed by the identity of their detailed $^{31}P$, $^{11}B$, and $^1H$ n.m.r. behaviour as summarized later in this paper.

The reaction between equimolar quantities of $[B_9H_{12}]^-$ and *trans*-$[Ir(CO)Cl(PMe_3)_2]$ in $CH_2Cl_2$ solution at ambient temperature is complete within a few minutes; the reaction may be essentially instantaneous but this is difficult to assess simply as there is no obvious colour change. Three major products are obtained, which may be separated chromatographically. These have been identified (see below) as the new nine-vertex *arachno*-iridanonaboranes [*asym*-4,4,4,4-(CO)-*endo*-H-*cis*-$(PMe_3)_2$-*arachno*-4-$IrB_8H_{12}$] (1) and [1-Cl-*sym*-4,4,4,4-(CO)-*endo*-H-*cis*-$(PMe_3)_2$-*arachno*-4-$IrB_8H_{11}$] (2), both colourless crystalline solids, and the known [5] yellow ten-vertex compound [6,6,6-$H(PMe_3)_2$-*nido*-6-$IrB_9H_{13}$]. At the scale the reaction was carried out (0.6 mmol), these were isolated in yields of 30, 7, and 5% respectively. Minor products (all ≤ *ca.* 1%) include a third new *arachno*-iridanonaborane [*sym*-4,4,4,4-*endo*-H-*mer*-$(PMe_3)_3$-*arachno*-4-$IrB_8H_{12}$] (3), and the previously reported [4] five-vertex *arachno*-iridapentaborane [1,1,1-$(CO)(PMe_3)_2$-*arachno*-1-$IrB_4H_9$] together with other smaller iridaboranes which we have not yet thoroughly characterized; n.m.r. evidence additionally suggests that trace quantities of other *arachno*-4-iridanonaborane variants may also be present. The mechanism of formation of these eight-boron iridanonaboranes from the nine-boron starting anion is at present unknown, but may be related to the high-yield formation [11] of the *arachno*-platinanonaborane $[(PtB_8H_{12})(PMe_2Ph)_2]$ from the nine-boron $[B_9H_{14}]^-$ anion and *cis*-$[PtCl_2(PMe_2Ph)_2]$.

The preliminary n.m.r. studies (subsequently extended and discussed in more detail below) of the new iridaboranes (1)—(3) suggested similar gross cluster geometries to that established for the *arachno*-platinanonaborane $[(PtB_8H_{12})(PMe_2Ph)_2]$ just mentioned above. That this is indeed the case was confirmed by single-crystal *X*-ray diffraction analysis for the chlorinated-*arachno*-iridanonaborane $[(HIrB_8H_{11}Cl)(CO)(PMe_3)_2]$ (2). A drawing of the molecular structure is shown in Figure 1, selected interatomic distances are given in Table 1, and selected angles between interatomic vectors are in Table 2.

The gross structural geometry is seen to be similar to that of the *arachno*-nonaborane *iso*-$B_9H_{15}$, with the metal atom in the 4-position. Hydrogen atoms were not located, but selective $^1H$-{$^{11}B$} n.m.r. spectroscopy showed that there is an *exo*-terminal hydrogen atom associated with each boron atom except B(1), that B(6) and B(8) each have in addition an *endo*-terminal hydrogen atom associated with them, and that there are two bridging hydrogen atoms, one between B(5) and B(6),

† *Supplementary data available* (No. SUP 23982, 17 pp.): thermal parameters, structure factors. See Instructions for Authors, *J. Chem. Soc., Dalton Trans.*, 1984, Issue 1, pp. xvii—xix.

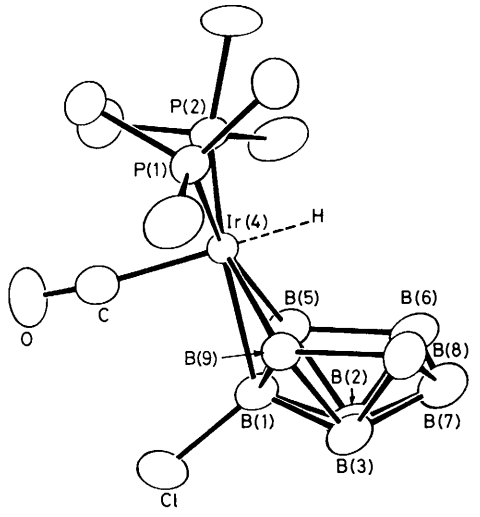


**Figure 1.** ORTEP drawing of the molecular structure of $[(HIrB_8H_{11}Cl)(CO)(PMe_3)_2]$ (2). Hydrogen atoms were not located, but the position of the Ir(4)–H terminal hydrogen atom evident from n.m.r. spectroscopy is indicated by a dashed line (see also Figure 2)

**Table 1.** Selected interatomic distances (pm) for $[(HIrB_8H_{11}Cl)(CO)(PMe_3)_2]$ (2), with estimated standard deviations in parentheses

| | | | |
|---|---|---|---|
| *(i)* From the iridium atom | | | |
| Ir(4)–B(5) | 228.4(11) | Ir(4)–B(9) | 229.1(8) |
| Ir(4)–B(1) | 226.1(10) | | |
| Ir(4)–P(1) | 233.4(2) | Ir(4)–P(2) | 234.6(2) |
| Ir(4)–C(carbonyl) | 193.4(10) | | |
| *(ii)* Boron–boron | | | |
| B(1)–B(2) | 173.9(15) | B(1)–B(3) | 178.1(14) |
| B(1)–B(5) | 181.0(15) | B(1)–B(9) | 177.5(13) |
| B(2)–B(3) | 176.8(13) | | |
| B(2)–B(5) | 181.6(15) | B(3)–B(9) | 181.4(13) |
| B(2)–B(6) | 174.7(15) | B(3)–B(8) | 176.7(16) |
| B(2)–B(7) | 177.5(18) | B(3)–B(7) | 177.4(16) |
| B(5)–B(6) | 191.1(15) | B(8)–B(9) | 189.9(14) |
| B(6)–B(7) | 179.4(15) | B(7)–B(8) | 187.9(15) |
| *(iii)* Other | | | |
| C–O(carbonyl) | 111.1(10) | | |
| B(1)–Cl | 184.6(10) | | |
| P(1)–C(methyl) | 180.0(10)—183.8(9) | | |
| P(2)–C(methyl) | 178.9(10)—181.9(9) | | |

**Table 2.** Selected angles (°) between interatomic vectors for $[(HIrB_8H_{11}Cl)(CO)(PMe_3)_2]$ (2), with estimated standard deviations in parentheses

| | | | |
|---|---|---|---|
| *(i)* At the iridium atom | | | |
| P(1)–Ir(4)–P(2) | 96.8(1) | | |
| P(1)–Ir(4)–C(carbonyl) | 92.2(3) | P(2)–Ir(4)–C(carbonyl) | 92.4(2) |
| P(1)–Ir(4)–B(1) | 130.7(3) | P(2)–Ir(4)–B(1) | 132.4(3) |
| P(1)–Ir(4)–B(5) | 166.3(3) | P(2)–Ir(4)–B(9) | 162.9(3) |
| P(1)–Ir(4)–B(9) | 87.4(2) | P(2)–Ir(4)–B(5) | 87.0(3) |
| C(carbonyl)–Ir(4)–B(1) | 86.5(3) | | |
| C(carbonyl)–Ir(4)–B(5) | 100.7(3) | C(carbonyl)–Ir(4)–B(9) | 104.0(3) |
| B(1)–Ir(4)–B(5) | 46.9(4) | B(1)–Ir(4)–B(9) | 45.9(3) |
| B(5)–Ir(4)–B(9) | 85.2(4) | | |
| *(ii)* Iridium–boron–boron | | | |
| Ir(4)–B(1)–B(2) | 119.5(6) | Ir(4)–B(1)–B(3) | 119.9(6) |
| Ir(4)–B(1)–B(5) | 67.2(5) | Ir(4)–B(1)–B(9) | 68.0(4) |
| Ir(4)–B(5)–B(1) | 65.9(4) | Ir(4)–B(9)–B(1) | 66.1(4) |
| Ir(4)–B(5)–B(2) | 114.9(6) | Ir(4)–B(9)–B(3) | 116.8(5) |
| Ir(4)–B(5)–B(6) | 116.9(6) | Ir(4)–B(9)–B(8) | 118.0(6) |
| *(iii)* Other | | | |
| Ir(4)–B(1)–Cl | 117.1(5) | | |
| B(5)–B(1)–Cl | 119.3(6) | B(9)–B(1)–Cl | 116.3(7) |
| B(2)–B(1)–Cl | 114.8(7) | B(3)–B(1)–Cl | 113.0(7) |
| Ir(4)–C–O(carbonyl) | 174.9(8) | | |
| B(5)–B(1)–B(9) | 119.5(7) | B(6)–B(7)–B(8) | 126.8(7) |
| Ir(4)–P(1)–C(methyl) | 114.6(3)—117.7(3) | | |
| Ir(4)–P(2)–C(methyl) | 114.9(3)—119.2(4) | | |

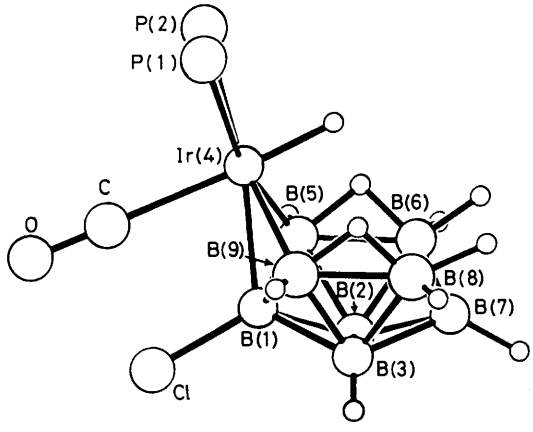


**Figure 2.** An alternative (schematic) view of the molecular structure of $[(HIrB_8H_{11}Cl)(CO)(PMe_3)_2]$ (2) with cluster hydrogen atoms (evident from n.m.r. spectroscopy) drawn in, but with P-methyl groups omitted. In this projection the *exo*-terminal hydrogen atom on B(2) is obscured

and one between B(8) and B(9). The n.m.r. showed that in addition there is a terminal hydrogen atom on iridium, *cis* to both the mutually *cis* phosphine ligands, as indicated by the broken line in Figure 1. Peaks corresponding to all these positions appeared in the final difference maps in the diffraction analysis. The disposition of the atoms, apart from those on the 4-position, is therefore as in the *arachno*-nine vertex analogues $[(PtB_8H_{12})(PMe_2Ph)_2]$,[11] and $B_9H_{13}(NCMe)$;[13] the positions are shown in Figure 2.

The boron–boron distances within the cage are within normal ranges, and the distances B(1)–B(5) and B(1)–B(9) of 181.0(15) and 177.5(13) pm, respectively, are similar to the corresponding distances[11] of 181(2) and 181(2) pm in $[(PtB_8H_{12})(PMe_2Ph)_2]$. The detailed geometry about the metal atom is of more interest and warrants a more detailed comparison with that of the platinum analogue however. Schematic representations of the geometry about the iridium atom in $[(HIrB_8H_{11}Cl)(CO)(PMe_3)_2]$ (2) together with that for the platinum compound $[(PtB_8H_{12})(PMe_2Ph)_2]$ for comparison are given in Figure 3.

The geometry about the iridium atom is interpretable in terms of an essentially octahedral disposition of bonding orbitals about an 18-electron iridium(III) metal centre; the tetragonal bonding plane defined by Ir(4)P(1)P(2) intersects the B(1)–B(5) and B(1)–B(9) vectors and so the dominant contributions to the borane-to-metal bonding presumably occur essentially *via* two two-electron bonds Ir(4)B(1)B(5) and Ir(4)B(1)B(9) which have both two- and three-centre charac-

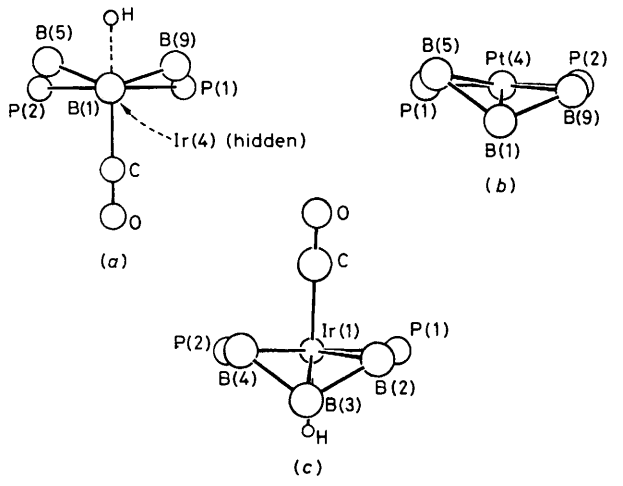


**Figure 3.** View along the P–M–P plane of the metal environment in (*a*) $[(HIrB_8H_{11}Cl)(CO)(PMe_3)_2]$ (2), (*b*) $[(PtB_8H_{12})(PMe_2Ph)_2]$ (data from ref. 11), and (*c*) $[(HIrB_3H_7)(CO)(PPh_3)_2]$ (data from J. Bould, N. N. Greenwood, J. D. Kennedy, and W. S. McDonald, unpublished work)

ter with analogies in classical π-allyl hydrocarbon ligation (see below). A valence-bond structure may be written down

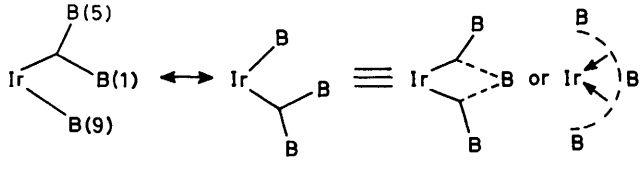


for this [Figure 4(*c*)] which is analogous to that generally held to obtain for $B_9H_{13}L$ species with 2613 *styx* topology [Figure 4(*c*)]. [Though this particular geometric disposition of atoms does not occur when L = $H^-$ (at least in the solid state, since the *X*-ray single-crystal structure of $[B_9H_{14}]^-$ reveals an alternative 2613 topology [14]) nevertheless it is well established for $B_9H_{13}(MeCN)$-4,[13] and the high degree of *endo*/bridging H-atom fluxionality indicates that the energetic differences are in any event small.] It may be noted that this borane-to-metal bonding scheme differs somewhat from that suggested for the so-called 'borallyl' iridium(v) complex $[(HIrB_3H_7)(CO)(PPh_3)_2]$: the borane-to-metal bonding in this smaller metallatetraborane in fact has closer analogies to that of another metallanonaborane, the previously described [11] nine-vertex *arachno*-platinaborane $[(PtB_8H_{12})(PMe_2Ph)_2]$ which is also included in Figure 3 and 4(*b*). In this platinum compound, the almost exact coplanarity of the Pt(4)P(1)P(2)B(5)B(9) atoms [Figure 3(*b*)] has been taken to indicate essentially $dsp^2$ hybridization involving direct two-electron two-centre bonds Pt(4)–B(5) and Pt(4)–B(9). In addition, metal 5*d* or *dp* electron-pair interaction with B(1) was postulated, implying the involvement of a third two-electron two-centre bond which in turn implies contributions from an effective platinum(IV) valency state.[11] The localized valence-bond structure for this [Figure 4(*b*)] is seen to be analogous to one of 2532 *styx* topology which may be written down for an *arachno*-nonaborane *iso*-$[B_9H_{13}]^{2-}$ anion. Significant contributions to the borane-to-metal bonding in this compound may therefore be regarded as occurring *via* three two-electron bonds, whereas in the iridium complex only two two-electron bonds need be invoked for this purpose. The topological representations in Figure 4(*a*) and 4(*b*) emphasize the important fact that in theory it is possible to alter the number of electrons which the metal vertex contributes to the cluster without radically altering the bonding within the remaining borane fragment.

These considerations have important manifestations in the application of the various skeletal bonding schemes to transition-metal containing metallaboranes. In the *arachno*-4-metallanonaboranes discussed here, the metal vertex notionally subrogates a $BH_2^-$ vertex in the formally isoelectronic borane clusters $[B_9H_{14}]^-$ and $[B_{10}H_{14}]^{2-}$ or a BHL vertex in $B_9H_{13}L$ and $B_{10}H_{12}L_2$. In Wade's terms these boron vertices contribute four electrons to the skeletal electron count since the bond to the *endo*-terminal hydrogen atom is regarded as contributing its electrons to the cluster. In Lipscomb's valence-bond approach the *endo*-terminal hydrogen actually subtracts an electron and an orbital from the cluster bonding, thereby effectively reducing the number of bonds remaining among the skeletal boron and bridging hydrogen atoms. In some compounds the former theory is also valid in terms of contributions to cluster bonding, since some boron hydrides such as *arachno*-$B_5H_{11}$ and *arachno*-$B_8H_{14}$ contain *endo*-terminal hydrogen atoms which have been shown by their $^1H$ n.m.r. spectra (and by an *X*-ray structural study for $B_5H_{11}$) to be bound to other cluster boron atoms. Consequently in these species the electron pair in the B–H(*endo*) bond may be regarded as delocalized into the cluster. Conversely, in *arachno*-$B_{10}H_{12}(SMe_2)_2$-6,9 and the *arachno*-platinanonaborane $[(PtB_8H_{12})(PMe_2Ph)_2]$ selective $^1H$-$\{^{11}B\}$ experiments have found that the *endo*-terminal hydrogens in these particular species have no pseudo-bridging character.[11,15] Thus the electron pairs in these *endo*-terminal B–H bonds do not necessarily play a role in the cluster bonding, although the compounds still feature *arachno* structures. Similarly, the terminal metal hydride in the *arachno*-iridanonaboranes reported here also does not feature any interaction with the cluster though it does occupy the position of the *endo*-terminal hydrogen atom in the analogous compound *arachno*-$B_9H_{13}L$. Thus it is not a necessary condition in *arachno*-clusters for the electrons in the *endo*-terminal bond to be involved in the cluster bonding proper to attain an *arachno*-structure and consequently there is no need to regard the iridium vertex in compounds (1)—(3) as an iridium(v) species, even though the platinum compound $[(PtB_8H_{12})(PMe_2Ph)_2]$ may have platinum(IV) character.

The orientations of the P(1)MP(2) planes for the compounds illustrated in Figure 3 emphasize that the bonding geometry in these types of cluster is highly variable and possibly, in these terms, reminiscent of 'slipped' *closo* bonding in some platinacarboranes in that many orientations of the P(1)MP(2) plane are possible within the basically similar cluster. The reasons for adopting any particular orientation may depend on such features as crystal-packing forces, contributions from nominally lone-pair electrons as in platinum(IV) structures, distortions arising from borane ligand or other ligand-sphere asymmetry, *etc.* In the case of compound (2), the observed geometry may be influenced by steric repulsion between the chlorine atom on B(1) and the carbonyl ligand causing a tilt in the P(1)Ir(4)P(2) plane towards B(1). In any event the result is that the iridanonaborane cluster, with an 18-electron iridium(III) centre, can be regarded as having a 22-electron skeletal *nido* bonding-electron count with an *arachno* structure.

These detailed bonding descriptions and intercomparisons are not inconsistent with the observed $^{11}B$ n.m.r. shielding behaviour of these species; data on this, together with cage-proton n.m.r. parameters, are summarized in Table 3. The $^{11}B$ n.m.r. spectrum of compound (1) is given in Figure 5. For the iridaborane n.m.r. parameters, assignments were made by

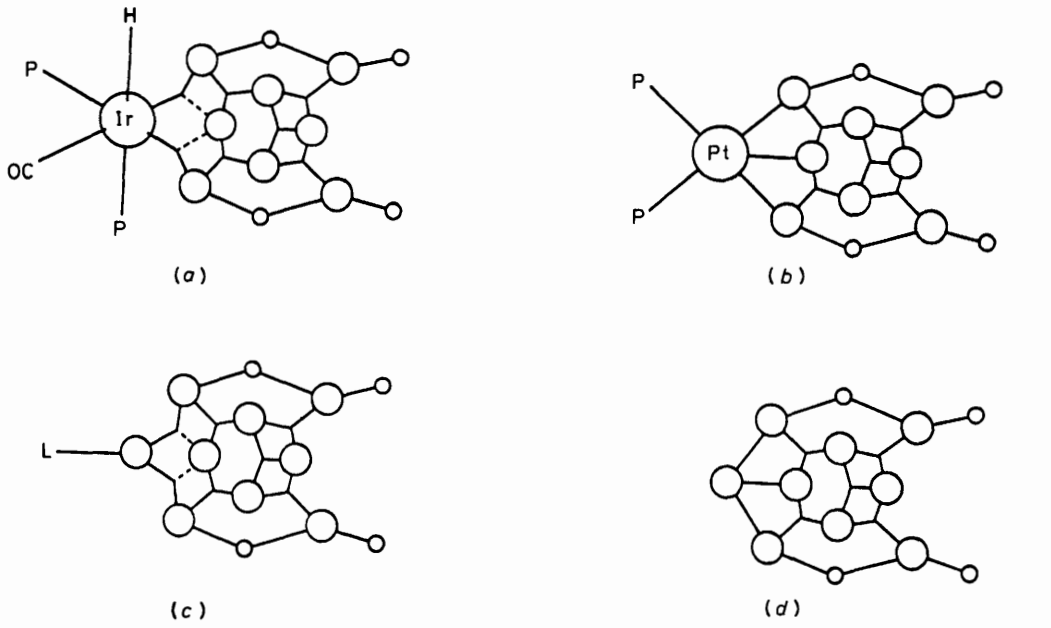


**Figure 4.** Valence-bond topological representations of supposed significant contributions to the skeletal bonding in (*a*) $[(HIrB_8H_{12})(CO)(PMe_3)_2]$ (1) and (*b*) the *arachno* platinanonaborane species $[(PtB_8H_{12})(PMe_2Ph)_2]$. Structures (*c*) and (*d*) represent respectively the appropriate valence-bond tautomers of what would be the corresponding non-metalla-species $B_9H_{13}L$-4 of effective 2613 *styx* topology and *arachno*-$[B_9H_{13}]^{2-}$ of presumed 2532 *styx* topology. In each case the semi-localized valence-bond structure depicted is one of a number of canonical forms which may be written down, and in each case there will be substantial electron delocalization over the cluster

peak multiplicities, *etc.*, comparison with the gross shielding behaviour of the previously assigned $[(PtB_8H_{12})(PMe_2Ph)_2]$ [11] and $B_9H_{13}L$ [16] species, and selective $^1H$-$\{^{11}B\}$ n.m.r. spectroscopy [11,17,18] which related those boron resonances designated B(5),B(9) and B(6),B(8) to the *endo*-terminal and bridging hydrogen atoms. With due allowance made in compound (2) for the known [19] deshielding effect of 10—20 p.p.m. for

**Table 3.** Boron-11 and proton n.m.r. data [a,b] for the polyhedral cages of $[(HIrB_8H_{12})(CO)(PMe_3)_2]$ (1), $[(HIrB_8H_{11}Cl)(CO)(PMe_3)_2]$ (2), and $[(HIrB_8H_{12})(PMe_3)_3]$ (3), with $B_9H_{13}(PMe_2Ph)$ and $[(PtB_8H_{12})(PMe_2Ph)_2]$ data for comparison; $CDCl_3$ solutions at +21 °C

| | Compound (1) | | Compound (2) | | Compound (3) | | $B_9H_{13}(PMe_2Ph)$ [c] | | $[(PtB_8H_{12})(PMe_2Ph)_2]$ [d] | |
|---|---|---|---|---|---|---|---|---|---|---|
| Position | δ(¹¹B) | δ(¹H) | δ(¹¹B) | δ(¹H) | δ(¹¹B) | δ(¹H) | δ(¹¹B) | δ(¹H) | δ(¹¹B) | δ(¹H) |
| (7) | +17.7 | +4.02 | +18.1 | +3.90 | +18.3 | +4.06 | +18.4 | +4.36 | +18.8 | +3.97 |
| (1) | +10.0 | +3.30 [e] | +24.1 | — [f] | +12.0 | +3.55 [g] | +3.4 | +3.14 | +21.6 | +4.20 |
| (5),(9) | −12.0 | +2.56 | −11.9 | +2.63 | −12.7 | +2.05 | −15.1 | +2.10 | −1.7 | +2.97 |
| | −13.3 | +1.98 | −11.9 | +2.63 | −12.7 | +2.05 | −15.1 | +2.10 | −1.7 | +2.97 |
| (6),(8) | −22.1 | +2.40, −0.24 | −24.0 | +2.34, −0.44 | −24.3 | +2.15, −0.78 | −21.8 | +2.12, +0.29 | −23.0 | +2.12, +0.25 |
| | −26.9 | +2.02, −0.42 | −24.0 | +2.34, −0.44 | −24.3 | +2.15, −0.78 | −21.8 | +2.12, +0.29 | −23.0 | +2.12, +0.25 |
| (2), (3) | −32.8 | +0.98 | −32.8 | +0.99 | −35.9 | +0.76 | −36.3 | +0.75 | −31.6 | +0.92 |
| | −40.5 | +0.50 | −32.8 | +0.99 | −35.9 | +0.76 | −36.3 | +0.75 | −31.6 | +0.92 |
| (5,6) (9,8) | — | −2.76, −3.80 | — | −3.09, −3.09 | — | −3.24, −3.24 | — | −3.09, −3.09 | — | −3.05, −3.05 |
| (4) | — | −16.08 [h] | — | −15.90 [i] | — | −17.65 [j] | −36.3 [k] | −0.18 [l] | — | — |

[a] δ(¹¹B) in p.p.m. ±0.5 to low field (high frequency) of $BF_3{\cdot}OEt_2$ (10% in $CDCl_3$) at +21 °C [Ξ 32 083 971 Hz]. [b] δ(¹H) in p.p.m. ±0.05 to low field (high frequency) of $SiMe_4$. [c] Data from N. N. Greenwood, M. J. Hails, J. D. Kennedy, and W. S. McDonald, *J. Chem. Soc., Dalton Trans.*, submitted for publication. [d] Data from ref. 11. [e] $^3J(^{31}P_{ax}–Ir–B–^1H)$ = 33 Hz. [f] Site of Cl substituent. [g] $^3J(^{32}P_{ax}–Ir–B–^1H)$ = 31.3 Hz. [h] $^2J(^{31}P–Ir–^1H)(cis)$ = 19 Hz; $^2J(^{31}P–Ir–^1H)(trans)$ = 148 Hz; $^4J(^1H–C–P–Ir–^1H)$(transoid) = 1.0 Hz. [i] Triplet, $^2J(^{31}P–Ir–^1H)$ = 18 Hz. [j] $^2J(^{31}P–Ir–^1H)(cis)$ = 17 Hz; $^2J(^{31}P–Ir–^1H)(trans)$ = 140 Hz; $^4J(^1H–C–P–Ir–^1H)$(transoid) = 0.9 ± 0.1 Hz. [k] $^1J(^{31}P–^{11}B)$ = 120 ± 8 Hz. [l] $^2J(^{31}P–B–^1H)$ = 9.8 ± 0.5 Hz.

**Table 4.** Phosphorus-31 and proton n.m.r. data [a] for the metal environment of $[(HIrB_8H_{12})(CO)(PMe_3)_2]$ (1), $[(HIrB_8H_{11}Cl)(CO)(PMe_3)_2]$ (2) and $[(HIrB_8H_{12})(PMe_3)_3]$ (3) in $CDCl_3$ solutions

| | Compound (1) | Compound (2) | Compound (3) |
|---|---|---|---|
| δ(³¹P)/p.p.m. [a,b] | −50.8(eq) [c] and −55.9(ax) | −52.9 (both eq) [d] | −53.5(eq) [d,e] −57.0(ax) [d,f] |
| $^2J(^{31}P–^{31}P)(cis)$/Hz [a] | 22 ± 2 | *g* | 21 ± 1 |
| δ(¹H)(PMe)/p.p.m. [h] | +1.50(ax), +1.83(eq) | +1.90 | +1.72(eq), +1.38(ax) [d,i] |
| $^2J(^{31}P–C–^1H)$/Hz | Both *ca.* 9 | 9.3 ± 0.5 | 8.3 ± 0.2(eq), 7.6 ± 0.2(ax) [d,i] |
| $^4J(^1H–Ir–P_{ax}–C–^1H)$(transoid)/Hz [d,j] | 1.0 ± 0.1 | — | 0.9 ± 0.1 |
| $^3J[^{31}P_{ax}–Ir–B(1)–^1H]$/Hz [d] | 33 ± 2 | — | 31.3 ± 1.0 |
| δ(¹H)(IrH)/p.p.m. [h] | −16.08 | −15.90 | −17.65 |
| $^2J(^{31}P_{ax}–Ir–^1H)(trans)$/Hz [d] | 148 ± 2 | — | 140 ± 2 |
| $^2J(^{31}P_{eq}–Ir–^1H)(cis)$/Hz [d] | 19 ± 1 | 18 ± 1 | 17 ± 1 |

[a] Proton data at +21 °C; phosphorus-31 data at −40 °C [compound (1)], −50 °C (2), and −65 °C (3). [b] ±0.02 p.p.m.; to low field (high frequency) of 85% $H_3PO_4$ (Ξ 40 480 730 Hz). [c] $w_{\frac{1}{2}}$ 61 Hz at +21 °C compared to $w_{\frac{1}{2}}$ of 34 Hz for peak at −55.9 p.p.m. Broadening due to coupling to boron, therefore assigned to $P_{eq}$ which is approximately *trans* to boron. [d] eq and ax $PMe_3$ groups are those so designated in the schematic representations of Figure 6. [e] Doublet, relative intensity 2, in $^{31}P-\{^1H$(broad band noise)$\}$ spectrum. [f] Triplet, relative intensity 1, in $^{31}P-\{^1H$(broad band noise)$\}$ spectrum. [g] Not directly measurable. [h] ±0.05 p.p.m.; to low field (high frequency) of $SiMe_4$. [i] eq : ax intensity ratio 2 : 1. [j] Confirmed by selective $^1H-\{^1H\}$ spectroscopy.

Selected $^{31}P$ and $^1H$ n.m.r. data for the three iridanonaboranes are summarized in Table 4. The overall $^{31}P$, $^{11}B$, and $^1H$ n.m.r. behaviour (Tables 3 and 4) for $[(HIrB_8H_{11}Cl)(CO)(PMe_3)_2]$ (2) is entirely consistent with the molecular structure as determined by *X*-ray diffraction (Figure 1), and conversely the ligand geometries about the metal atoms in $[(HIrB_8H_{12})(CO)(PMe_3)_2]$ (1) and $[(HIrB_8H_{12})(PMe_3)_3]$ (3) readily follow from consideration of the n.m.r. data. The n.m.r. data for compound (1) indicate an asymmetric molecule which, as the borane cage is unsubstituted, must be due to the arrangement of ligands about the iridium. It is reasonable to assume that the ligands are in a pseudo-octahedral arrangement similar to that for compound (2). Low-temperature $^{31}P$ n.m.r. spectroscopy (*i.e.* with the phosphorus nuclei 'thermally decoupled' from boron [20]) shows two sharp doublets with $^2J(^{31}P–^{31}P)$ of 22 Hz indicative of two *cis*-phosphines. At ambient temperature one resonance remains relatively sharp ($w_{\frac{1}{2}}$ 34 Hz) whereas the other broadens ($w_{\frac{1}{2}}$ 61 Hz), due to marked coupling to boron, thereby enabling the latter phosphine to be assigned an equatorial position *trans* to the borane cage whereas the former phosphine is in a *cis*-axial position. The $^1H$ n.m.r. spectrum shows a metal hydride coupled to one *cis*-phosphine $[^2J(^{31}P–^1H)(cis)$ 19 Hz] and one *trans*-phosphine $[^2J(^{31}P–^1H)$ (*trans*) 148 Hz] thus placing it in an axial position *trans* to the axial phosphine. The asymmetry of the molecule is introduced by the carbonyl group, shown to be present from the infrared spectrum [$\nu_{max.}$(CO) 2 000 $cm^{-1}$], which must reside in the remaining equatorial position. In compound (3) similar arguments apply except that now the $^{31}P$ n.m.r. spectrum exhibits three *cis* phosphines in the ratio of 2 : 1 with the $^{11}B$ and $^1H$ n.m.r. indicating a molecule with a plane of symmetry. Thus the carbonyl position in compound (1) is occupied by the third phosphine in compound (3). The structures thus established are summarized in Figure 6, which enables the descriptions thus required, *viz.*, [*asym*-4,4,4,4-(CO)-*endo*-H-*cis*-$(PMe_3)_2$-*arachno*-4-$IrB_8H_{12}$] (1), [1-Cl-*sym*-4,4,4,4-(CO)-*endo*-H-*cis*-$(PMe_3)_2$-*arachno*-4-$IrB_8H_{11}$] (2), and [*sym*-4,4,4,4-*endo*-H-*mer*-$(PMe_3)_3$-*arachno*-4-$IrB_8H_{12}$] (3), to be more interpretable. The H(*endo*) *trans* to P(axial) [rather than a P atom in the *endo* position *trans* to H(*exo*/axial)] configurations are ascribed to compounds (1) and (3) on the basis of analogy with compound (2), and on the prohibitive steric hindrance that would arise with a 13-atom $PMe_3$ group in the *endo* position. In this context the large vicinal *cisoid* coupling $^2J(^{31}P–Ir–B–^1H)$ between the eclipsed P(axial) and the H(1) nuclei is at first sight unexpectedly large but has precedent [6] in a similar coupling $^3J(^{31}P–^1H)$ of 33 Hz between the nuclei of the eclipsed P(1) and H(4) atoms in the *exo*-bicyclic species $[\{o\text{-}(Ph_2P)C_6H_4\}_2(Ir_2B_4H_2)(CO)_3(PPh_3)]$. Additional points of

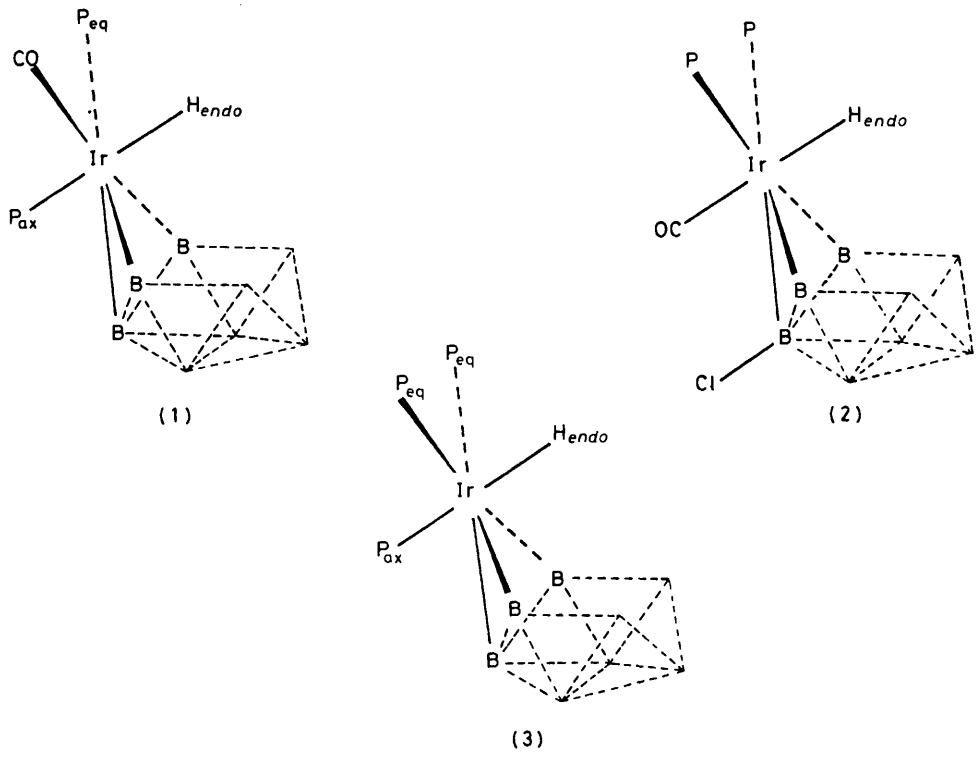


**Figure 6.** Schematic representation of the bonding geometries about the iridium atom in $[(HIrB_8H_{12})(CO)(PMe_3)_2]$ (1), $[(HIrB_8H_{11}Cl)(CO)(PMe_3)_2]$ (2), and $[(HIrB_8H_{12})(PMe_3)_3]$ (3). That of compound (2) is as established by *X*-ray diffraction analysis (Figure 1) and those for compounds (1) and (3) arise from consideration of the n.m.r. properties as summarized in Tables 3 and 4

interest arising from the n.m.r. spectra include the observation of the small transoid couplings $^4J[^1H(exo)\text{–}Ir\text{–}P\text{–}C\text{–}^1H]$ of *ca.* 1 Hz in compounds (1) and (3), and the observation that the asymmetry induced by the differential *trans* effects of the $PMe_3$ and CO ligands in compound (1) are more manifest in the $^{11}B$ shieldings of the *next* nearest neighbours in the B(6), B(8) and B(2),B(3) positions. It is interesting to speculate whether this last arises from a greater electronic change at these more distant positions, or from a greater sensitivity of the shielding tensor at these positions to small electronic changes.

The nature of the products (Figure 6) perhaps warrants a brief further discussion. As mentioned in the opening paragraphs, the mechanism of the reaction between $[B_9H_{12}]^-$ and *trans*-$[Ir(CO)Cl(PMe_3)_2]$ is unknown, but the fact that the major product [compound (1), 30% yield] contains no halogen and retains the $(CO)(PMe_3)_2$ ligation of the starting complex may argue for an initial straightforward metathesis which would then be followed by the elimination of a boron vertex; however, the presence of the 1-chloro-substituent in compound (2) could also indicate an initial additive process; and it is evident from compound (3), and also the isolation of $B_9H_{13}(PMe_3)$ from closely related systems,[5] that ligand dissociation is also of significance. It is also of interest that when $[IrCl(PPh_3)_3]$ is used as a starting substrate with $[B_9H_{12}]^-$ then little, if any, cage degradation occurs to form $IrB_8$ clusters and the *exo* cyclic ten-vertex species $[\{(o\text{-}Ph_2P)C_6H_4\}(HIrB_9H_{12})(PPh_3)]$ are formed in the high yield of 87%.[7]

## Experimental

*General.*—Metal starting complexes were prepared by standard methods and the $[B_9H_{12}]^-$ salt $[NEt_4][B_9H_{12}]$ was prepared as described in the literature.[21] Incidental to this work we recorded the $^1H$ n.m.r. spectrum of the $[B_9H_{12}]^-$ anion, and related the resonances to those of the nuclei of the directly bonded B atoms by selective $^1H\text{-}\{^{11}B\}$ spectroscopy. The $^1H$ spectrum of this species was previously unreported, and will be summarized in more detail in a forthcoming paper.[22] Reactions were carried out, and solids and solutions kept, under an atmosphere of dry nitrogen, although manipulations and separatory procedures were usually carried out in air. Preparative and analytical thin-layer chromatography (t.l.c.) were carried out using silica gel G with a fluorescence indicator (Fluka type GF 254) as the stationary phase, using general procedures described in more detail in previous papers;[11,23,24] components were detected visually by ambient light and by observation of fluorescence under u.v. irradiation. Infrared spectra were recorded on a Perkin-Elmer 457 instrument and values quoted are $\pm 5$ $cm^{-1}$. Mass spectra were recorded using an AEI/Kratos MS 30 instrument using electron-impact ionization at 70 eV.

*N.M.R. Spectroscopy.*—100-MHz $^1H$, 40-MHz $^{31}P$, and 32-MHz $^{11}B$ n.m.r. spectroscopy was carried out using a JEOL FX-100 instrument. $^{31}P\{^1H(broad\ band\ noise)\}$ spectra were generally recorded at low temperatures to maximize line-sharpening arising from the 'thermal decoupling' of boron nuclear spins.[20] Selective $^1H\text{-}\{^{11}B\}$ double-resonance experiments were carried out as previously described;[11,17,18] power levels used for these experiments were of the order $\gamma B_2/2\pi = 500$ Hz, this value being estimated on the basis of off-resonance residual splittings as described elsewhere.[25] 128-MHz $^{11}B$ spectroscopy was carried out using the SERC Bruker WH400 instrument at the University of Sheffield.

*Reaction of* $[NEt_4][B_9H_{12}]$ *with* trans-$[Ir(CO)Cl(PMe_3)_2]$.—To a stirred solution of $[NEt_4][B_9H_{12}]$ (150 mg, 0.6 mmol) in $CH_2Cl_2$ (30 $cm^3$) at ambient temperature was added *trans*-$[Ir(CO)Cl(PMe_3)_2]$ (240 mg, 0.6 mmol); the ensuing reaction appeared to be instantaneous, but there were no colour changes by which to judge this accurately. The solution was filtered, and concentrated under reduced pressure (rotary evaporator, *ca.* 45 °C). Preparative t.l.c. yielded three bands (designated here by the letters A—C) of which two consisted of single components; $R_f$ values using 70% $CH_2Cl_2$—30% light petroleum (b.p. 40—60 °C) as the liquid phase were as follows: component A, $R_f$ 0.45, 18 mg, colourless solid, located under u.v. light; component B, $R_f$ 0.5, 13 mg, yellow solid; and band C, $R_f$ *ca.* 0.8. Band C contained many components and was therefore rechromatographed using 50% $CH_2Cl_2$—50% pentane as liquid phase, and three further components were isolated (D—F): component D, $R_f$ 0.6, 3 mg, colourless solid located under u.v. light; component E, $R_f$ 0.7, 72 mg, colourless solid located under u.v. light, and component F, $R_f$ 0.8, 2 mg, pale yellow solid. Component B was identified by $^1H$, $^{11}B$, and $^{31}P$ single and multiple resonance n.m.r. spectroscopy as the previously reported [5] *nido*-6-iridadecaborane $[(HIrB_9H_{13})(PMe_3)_2]$, yield 5%. The component F has been characterized as described elsewhere [4] as the *arachno*-1-iridapentaborane $[(IrB_4H_9)(CO)(PMe_3)_2]$, yield ≤ *ca.* 1%. Components E, A, and D were characterized as the *arachno*-4-iridanonaboranes (1), (2), and (3) as discussed in the text; $^{11}B$, $^1H$, and $^{31}P$ n.m.r. data are given in Tables 3 and 4; additional data are as follows. Component E [compound (1)] was a colourless crystalline solid, yield 30%, m.p. (decomp.) *ca.* 160 °C, $\nu_{max.}$(CO) 2 000, $\nu_{max.}$(Ir–H) 2 060 $cm^{-1}$ (Found: C, 18.9; H, 6.45. $C_7H_{31}B_8IrOP_2$ requires C, 17.9; H, 6.55%), *m/e* (max.) 472, $^{12}C_7{}^1H_{31}{}^{11}B_8{}^{193}Ir^{16}O^{31}P_2$ requires 474, indicating facile loss of $H_2$ from molecular ion (see ref. 22); the fragmentation also indicated facile loss of CO. Component A [compound (2)] was a colourless crystalline solid, m.p. (decomp.) 140—150 °C, yield 7%, $\nu_{max.}$(CO) 1 990, $\nu_{max.}$(Ir–H) 2 100 $cm^{-1}$; insufficient quantities of rigorously purified sample were available for conventional elemental analysis, but the constitution of the compound was confirmed by single-crystal *X*-ray diffraction analysis as described below and in the text. That the crystal was representative of the bulk sample follows reasonably from the n.m.r. properties. Component D [compound (3)] was also a colourless crystalline solid, yield ~1%; elemental analysis was precluded because only trace amounts of this component were present, but its identity readily followed from n.m.r. spectroscopy as discussed in the text.

*X-Ray Diffraction Analysis.*—Recrystallization of $[(HIrB_8H_{11}Cl)(CO)(PMe_3)_2]$ (2) from dichloromethane–light petroleum (b.p. 40—60 °C) yielded colourless crystals suitable for single-crystal *X*-ray diffraction analysis.

*Crystal data.* $C_7H_{30}B_8ClIrOP_2$, $M$ = 506.4, monoclinic, $a$ = 971.9(2), $b$ = 2 423.9(4), $c$ = 955.0(2) pm, $\beta$ = 117.80(2)°, $U$ = 1.990 2(6) $nm^3$, $Z$ = 4, $D_c$ = 1.690 g $cm^{-3}$, $F(000)$ = 976, space group $P2_1/c$, Mo-$K_\alpha$ radiation, graphite monochromatized, $\lambda$ = 71.069 pm, $\mu$(Mo-$K_\alpha$) = 69.66 $cm^{-1}$.

*Structure determination.* Measurements were made on a Syntex $P2_1$ diffractometer. Cell dimensions and their standard deviations were obtained by least-squares treatment of the setting angles of 15 reflections having $35 < 2\theta < 40°$. Intensities for all independent reflections with $4 < 2\theta < 45°$ were measured in the $\omega$—$2\theta$ scan mode, with scans running from 1° below $\alpha_1$ to 1° above $\alpha_2$. Variable scan speeds (according to a pre-scan intensity) of 4—29° $min^{-1}$ were used; under these conditions a control reflection showed negligible decline in intensity. After correction for Lorentz, polarization, and transmission factors [range 6.8—10.7], those reflections (2 430) having $I > 2\sigma(I)$ were retained for the structure analysis; 194 below this threshold were rejected as 'unobserved'. The structure was solved from Patterson and difference syntheses; full-matrix least-squares refinement with anisotropic thermal parameters for non-hydrogen atoms converged at $R$ = 0.053, $R'$ = 0.092.

Computations used the SHELX programs throughout and this allowed the methyl hydrogens to be included as part of a rigid regular tetrahedron with C–H = 108 pm and $U_{iso}$ for the H atoms of 700 $pm^2$. Least-squares weights were obtained from the modified variances $\sigma^2(I) = \sigma_c^2(I) + (0.02I)^2$ and the final $R$ was 0.034, $R'$ = 0.057. Peaks corresponding to all those borane hydrogens observed in the $^1H$ n.m.r. appeared on a difference map, but these could not be refined satisfactorily and were therefore omitted. The final atomic co-ordinates and their estimated standard deviations are given in Table 5.

**Table 5.** Fractional co-ordinates for $[(HIrB_8H_{11}Cl)(CO)(PMe_3)_2]$ (2)

| Atom | *x* | *y* | *z* |
|---|---|---|---|
| Ir | 0.268 86(3) | 0.111 81(1) | 0.058 03(3) |
| P(1) | 0.532 3(2) | 0.135 1(1) | 0.182 2(2) |
| P(2) | 0.252 5(2) | 0.088 8(1) | 0.288 5(2) |
| Cl | 0.079 9(2) | 0.049 5(1) | −0.316 5(2) |
| C | 0.312 6(9) | 0.036 4(3) | 0.025 5(8) |
| O | 0.345 5(8) | −0.007 0(2) | 0.018 2(8) |
| B(1) | 0.091 2(11) | 0.111 9(3) | −0.200 8(12) |
| B(9) | 0.248 2(11) | 0.157 5(3) | −0.161 0(9) |
| B(5) | 0.003 2(12) | 0.111 3(3) | −0.070 4(13) |
| B(6) | −0.098 6(12) | 0.181 2(4) | −0.107 9(12) |
| B(2) | −0.084 6(11) | 0.146 2(4) | −0.260 7(11) |
| B(7) | −0.039 8(12) | 0.217 7(6) | −0.234 8(12) |
| B(3) | 0.053 3(11) | 0.173 8(4) | −0.313 4(12) |
| B(8) | 0.164 9(12) | 0.230 0(4) | −0.199 1(12) |
| C(11) | 0.661 9(9) | 0.081 8(3) | 0.315 0(11) |
| H(111) | 0.622 6(9) | 0.070 1(3) | 0.399 7(11) |
| H(112) | 0.779 0(9) | 0.097 7(3) | 0.377 0(11) |
| H(113) | 0.660 3(9) | 0.046 1(3) | 0.246 6(11) |
| C(12) | 0.585 3(12) | 0.197 0(4) | 0.299 7(12) |
| H(121) | 0.536 2(12) | 0.196 2(4) | 0.380 5(12) |
| H(122) | 0.541 0(12) | 0.232 4(4) | 0.222 7(12) |
| H(123) | 0.710 4(12) | 0.199 8(4) | 0.366 1(12) |
| C(13) | 0.626 1(9) | 0.145 7(4) | 0.056 8(12) |
| H(131) | 0.563 5(9) | 0.176 8(4) | −0.031 2(12) |
| H(132) | 0.625 9(9) | 0.107 5(4) | −0.001 4(12) |
| H(133) | 0.744 6(9) | 0.159 1(4) | 0.129 1(12) |
| C(21) | 0.067 7(11) | 0.102 0(4) | 0.286 8(12) |
| H(211) | −0.025 8(11) | 0.084 2(4) | 0.182 0(12) |
| H(212) | 0.050 4(11) | 0.146 0(4) | 0.287 2(12) |
| H(213) | 0.068 9(11) | 0.083 9(4) | 0.390 8(12) |
| C(22) | 0.284 2(12) | 0.017 5(3) | 0.342 3(12) |
| H(221) | 0.213 4(12) | −0.007 6(3) | 0.240 4(12) |
| H(222) | 0.252 9(12) | 0.009 5(3) | 0.435 1(12) |
| H(223) | 0.405 4(12) | 0.007 5(3) | 0.384 0(12) |
| C(23) | 0.379 6(12) | 0.122 7(4) | 0.471 7(12) |
| H(231) | 0.498 6(12) | 0.118 9(4) | 0.493 5(12) |
| H(232) | 0.367 2(12) | 0.163 7(4) | 0.567 6(12) |
| H(233) | 0.348 7(12) | 0.165 8(4) | 0.464 0(12) |

## Acknowledgements

We thank the S.E.R.C. for support, and for maintenance grants (to J. B. and J. E. C.), and Dr. W. S. McDonald for very helpful collaboration [10] in the *X*-ray diffraction work.

## References

1 N. N. Greenwood, J. D. Kennedy, W. S. McDonald, D. Reed, and J. Staves, *J. Chem. Soc., Dalton Trans.*, 1979, 117.

2 N. N. Greenwood, J. D. Kennedy, and D. Reed, *J. Chem. Soc., Dalton Trans.*, 1980, 196.
3 J. E. Crook, N. N. Greenwood, J. D. Kennedy, and W. S. McDonald, *J. Chem. Soc., Chem. Commun.*, 1981, 933.
4 J. Bould, N. N. Greenwood, and J. D. Kennedy, *J. Chem. Soc., Dalton Trans.*, 1982, 481.
5 S. K. Boocock, J. Bould, N. N. Greenwood, J. D. Kennedy, and W. S. McDonald, *J. Chem. Soc., Dalton Trans.*, 1982, 713.
6 J. E. Crook, N. N. Greenwood, J. D. Kennedy, and W. S. McDonald, *J. Chem. Soc., Chem. Commun.*, 1982, 383.
7 J. Bould, N. N. Greenwood, J. D. Kennedy, and W. S. McDonald, *J. Chem. Soc., Chem. Commun.*, 1982, 465.
8 J. E. Crook, N. N. Greenwood, J. D. Kennedy, and W. S. McDonald, *J. Chem. Soc., Chem. Commun.*, 1983, 83.
9 J. Bould, N. N. Greenwood, and J. D. Kennedy, *J. Organomet. Chem.*, 1983, **249**, 11.
10 J. Bould, J. E. Crook, N. N. Greenwood, J. D. Kennedy, and W. S. McDonald, *J. Chem. Soc., Chem. Commun.*, 1982, 346.
11 S. K. Boocock, N. N. Greenwood, M. J. Hails, J. D. Kennedy, and W. S. McDonald, *J, Chem. Soc., Dalton Trans.*, 1981, 1415.
12 See R. M. Adams, *Pure Appl. Chem.*, 1972, **30**, 683.
13 F. E. Wang, P. G. Simpson, and W. N. Lipscomb, *J. Chem. Phys.*, 1961, **35**, 1335.
14 N. N. Greenwood, J. A. McGinnety, and J. D. Owen, *J. Chem. Soc., Dalton Trans.*, 1972, 986.
15 J. E. Crook, N. N. Greenwood, J. D. Kennedy, and W. S. McDonald, *J. Chem. Soc., Dalton Trans.*, in the press.
16 G. M. Bodner, F. R. Scholer, L. J. Todd, K. E. Senor, and J. C. Carter, *Inorg. Chem.*, 1977, **10**, 942.
17 J. D. Kennedy and N. N. Greenwood, *Inorg. Chim. Acta*, 1980, **38**, 93.
18 J. D. Kennedy and B. Wrackmeyer, *J. Magn. Reson.*, 1980, **38**, 529.
19 R. Ahmad, Ph.D. Thesis, University of Leeds, 1982; R. Ahmad, N. N. Greenwood, and J. D. Kennedy, unpublished work.
20 J. D. Kennedy and J. Staves, *Z. Naturforsch., Teil. B*, 1979, **34**, 808.
21 B. M. Graybill, J. K. Ruff, and M. F. Hawthorne, *J. Am. Chem. Soc.*, 1961, **83**, 2669.
22 J. Bould, N. N. Greenwood, and J. D. Kennedy, *J. Chem. Soc., Dalton Trans.*, in the press.
23 S. K. Boocock, N. N. Greenwood, J. D. Kennedy, W. S. McDonald, and J. Staves, *J. Chem. Soc., Dalton Trans.*, 1980, 790.
24 S. K. Boocock, N. N. Greenwood, J. D. Kennedy, W. S. McDonald, and J. Staves, *J. Chem. Soc., Dalton Trans.*, 1981, 2573.
25 T. C. Gibb and J. D. Kennedy, *J. Chem. Soc., Faraday Trans. 2*, 1982, 525.

*Received 24th November* 1983; *Paper* 3/2089